Two-mode model for metal-dielectric guided-mode resonance filters

Christelle Tuambilangana, Fabrice Pardo, Emilie Sakat, Patrick Bouchon, Jean-Luc Pelouard, Riad Haïdar

Two-mode model for metal-dielectric guided-mode resonance filters

Christelle Tuambilangana,[1,2] **Fabrice Pardo,**[2,*] **Emilie Sakat,**[1,2] **Patrick Bouchon,**[1] **Jean-Luc Pelouard,**[2] **and Riad Haïdar**[1]

[1]*MiNaO Joint Lab., ONERA-The French Aerospace Lab, F-91761 Palaiseau, France*
[2]*MiNaO Joint Lab., LPN, CNRS, Université Paris-Saclay, route de Nozay, F-91460 Marcoussis, France*
[*]*fabrice.pardo@lpn.cnrs.fr*

Abstract: Symmetric metal-dielectric guided-mode resonators (GMR) can operate as infrared band-pass filters, thanks to high-transmission resonant peaks and good rejection ratio. Starting from matrix formalism, we show that the behavior of the system can be described by a two-mode model. This model reduces to a scalar formula and the GMR is described as the combination of two independent Fabry-Perot resonators. The formalism has then been applied to the case of asymmetric GMR, in order to restore the properties of the symmetric system. This result allows designing GMR-on-substrate as efficient as free-standing systems, the same high transmission maximum value and high quality factor being conserved.

OCIS codes: (130.7408) Wavelength filtering devices; (310.2790) Guided waves (050.2230) Fabry-Perot; (310.6628) Subwavelength structures, nanostructures; (310.6805) Theory and design; (350.2460) Filters, interference.

References and links

1. T. W. Ebbesen, H. Lezec, H. Ghaemi, T. Thio, and P. Wolff, "Extraordinary optical transmission through subwavelength hole arrays," Nature **391**, 667–669 (1998).
2. H. Ghaemi, T. Thio, D. E. Grupp, T. W. Ebbesen, and H. Lezec, "Surface plasmons enhance optical transmission through subwavelength holes," Phys. Rev. B **58**, 6779 (1998).
3. T. J. Kim, T. Thio, T. W. Ebbesen, D. E. Grupp, and H. J. Lezec, "Control of optical transmission through metals perforated with subwavelength hole arrays," Opt. Lett. **24**, 256–258 (1999).
4. S. Lal, S. Link, and N. J. Halas, "Nano-optics from sensing to waveguiding," Nat. Photonics **1**, 641–648 (2007).
5. J. N. Anker, W. P. Hall, O. Lyandres, N. C. Shah, J. Zhao, and R. P. Van Duyne, "Biosensing with plasmonic nanosensors," Nat. Mater. **7**, 442–453 (2008).
6. J. A. Schuller, E. S. Barnard, W. Cai, Y. C. Jun, J. S. White, and M. L. Brongersma, "Plasmonics for extreme light concentration and manipulation," Nat. Mater. **9**, 193–204 (2010).
7. H. A. Atwater and A. Polman, "Plasmonics for improved photovoltaic devices," Nat. Mater. **9**, 205–213 (2010).
8. J. Porto, F. García-Vidal, and J. Pendry, "Transmission resonances on metallic gratings with very narrow slits," Phys. Rev. Lett. **83**, 2845 (1999).
9. R. Haïdar, G. Vincent, S. Collin, N. Bardou, N. Guérineau, J. Deschamps, and J.-L. Pelouard, "Free-standing subwavelength metallic gratings for snapshot multispectral imaging," Appl. Phys. Lett. **96**, 221104 (2010).
10. E. Sakat, G. Vincent, P. Ghenuche, N. Bardou, S. Collin, F. Pardo, J.-L. Pelouard, and R. Haïdar, "Guided mode resonance in subwavelength metallodielectric free-standing grating for bandpass filtering," Opt. Lett. **36**, 3054–3056 (2011).
11. E. Sakat, G. Vincent, P. Ghenuche, N. Bardou, C. Dupuis, S. Collin, F. Pardo, R. Haïdar, and J.-L. Pelouard, "Free-standing guided-mode resonance band-pass filters: from 1d to 2d structures," Opt. Express **20**, 13082–13090 (2012).
12. C.-H. Park, Y.-T. Yoon, and S.-S. Lee, "Polarization-independent visible wavelength filter incorporating a symmetric metal-dielectric resonant structure," Opt. Express **20**, 23769–23777 (2012).

#246738 Received 24 Jul 2015; revised 11 Oct 2015; accepted 19 Oct 2015; published 30 Nov 2015

13. E. Sakat, S. Héron, P. Bouchon, G. Vincent, F. Pardo, S. Collin, J.-L. Pelouard, and R. Haïdar, "Metal-dielectric bi-atomic structure for angular-tolerant spectral filtering," Opt. Lett. **38**, 425–427 (2013).
14. J. Le Perchec, R. E. de Lamaestre, M. Brun, N. Rochat, O. Gravrand, G. Badano, J. Hazart, and S. Nicoletti, "High rejection bandpass optical filters based on sub-wavelength metal patch arrays," Opt. Express **19**, 15720–15731 (2011).
15. S. S. Wang, M. G. Moharam, R. Magnusson, and J. S. Bagby, "Guided-mode resonances in planar dielectric-layer diffraction gratings," J. Opt. Soc. Am. A **7**, 1470–1474 (1990).
16. R. Magnusson and S. S. Wang, "New principle for optical filters," Appl. Phys. Lett. **61**, 1022–1024 (1992).
17. P. Lalanne, J.-P. Hugonin, S. Astilean, M. Palamaru, and K. D. Möller, "One-mode model and airy-like formulae for one-dimensional metallic gratings," J. Opt. A: Pure Appl. Opt. **2**, 48 (2000).
18. S. Collin, F. Pardo, and J.-L. Pelouard, "Waveguiding in nanoscale metallic apertures," Opt. Express **15**, 4310–4320 (2007).
19. B. Portier, F. Pardo, P. Bouchon, R. Haïdar, and J.-L. Pelouard, "Fast modal method for crossed grating computation, combining finite formulation of maxwell equations with polynomial approximated constitutive relations," J. Opt. Soc. Am. A **30**, 573–581 (2013).
20. C. Koechlin, P. Bouchon, F. Pardo, J. Jaeck, X. Lafosse, J.-L. Pelouard, and R. Haïdar, "Total routing and absorption of photons in dual color plasmonic antennas," Appl. Phys. Lett. **99**, 241104 (2011).
21. R. L. Olmon, B. Slovick, T. W. Johnson, D. Shelton, S.-H. Oh, G. D. Boreman, and M. B. Raschke, "Optical dielectric function of gold," Phys. Rev. B **86**, 235147 (2012).
22. P. T. Leung, S. Y. Liu, and K. Young, "Completeness and orthogonality of quasinormal modes in leaky optical cavities," Phys. Rev. A **49**, 3057–3067 (1994).
23. R. K. Chang and A. J. Campillo, *Optical Processes in Microcavities* (World Scientific, 1996).
24. B. E. A. Saleh and M. C. Teich, *Fundamentals of Photonics* (John Wiley & Sons, Inc., 2001).
25. T. Estruch, J. Jaeck, F. Pardo, S. Derelle, J. Primot, J.-L. Pelouard, and R. Haïdar, "Perfect extinction in subwavelength dual metallic transmitting gratings," Opt. Lett. **36**, 3160–3162 (2011).
26. V. Karagodsky, C. Chase, and C. J. Chang-Hasnain, "Matrix fabry-perot resonance mechanism in high-contrast gratings," Opt. Lett. **36**, 1704–1706 (2011).
27. C.J. Chang-Hasnain and W. Yang, "High-contrast gratings for integrated optoelectronics," Adv. Opt. Photonics **4**, 379–440 (2012).

1. Introduction

Metal-based nanostructured thin films have received a growing interest since the first theoretical and experimental evidences of extraordinary transmission [1–3]. This phenomenon originates from the coupling of the incident light to surface plasma waves and has been applied to various fields of research like microfluidic, photovoltaic devices [4–7]. Metallic gratings with narrow slits have been shown to exhibit high transmission [8] and can be used as an alternative to thin films for infrared band-pass filters, especially in the case of multispectral imaging [9]. More recently, metal-dielectric guided mode resonances (GMR) filters have been introduced [10]. They permit to design unpolarized filters [11, 12] or high angular tolerance filters [13] with an improved rejection ratio away from resonance. Nonetheless, one of the main drawback of these devices is that they are based on membranes, which complicates their fabrication and decreases their mechanical robustness. One solution consists in using a substrate [14]. However, in most of the cases, the introduction of a dissymetry between the top and the bottom interfaces of these filters is to the detriment of its performances. Likewise, for lossless Fabry-Perot filters, 100% transmission are only reached for symmetric filters.

In this article, we develop a two modes model that accurately accounts for the various resonance peaks of metal-dielectric GMR filters, highlighting the paramount influence of the 0^{th} and $\pm 1^{\text{st}}$ orders in the resonance mechanism. This model is further simplified to give a scalar expression of the transmitted intensity, and the GMR can be described by two coupled resonators. By analogy with a Fabry-Perot resonator, a symmetrisation criterion is formulated thanks to the scalar expression for either one of the coupled states. We show in the case of a GMR on substrate filter, that it is possible to satisfy this criterion for the first resonator and to restore the same performances than the symmetric filter.

First, we introduce the matrix formalism to compute the transmission spectra of the metal-

#246738 Received 24 Jul 2015; revised 11 Oct 2015; accepted 19 Oct 2015; published 30 Nov 2015

dielectric GMR filters, and show that it can be reduced to a two modes model. It can be further simplified to a two terms scalar expression for the transmission. In the Sec. 3, we use this expression to formulate a symmetrisation criterion and apply it to various cases of asymmetric GMR filters.

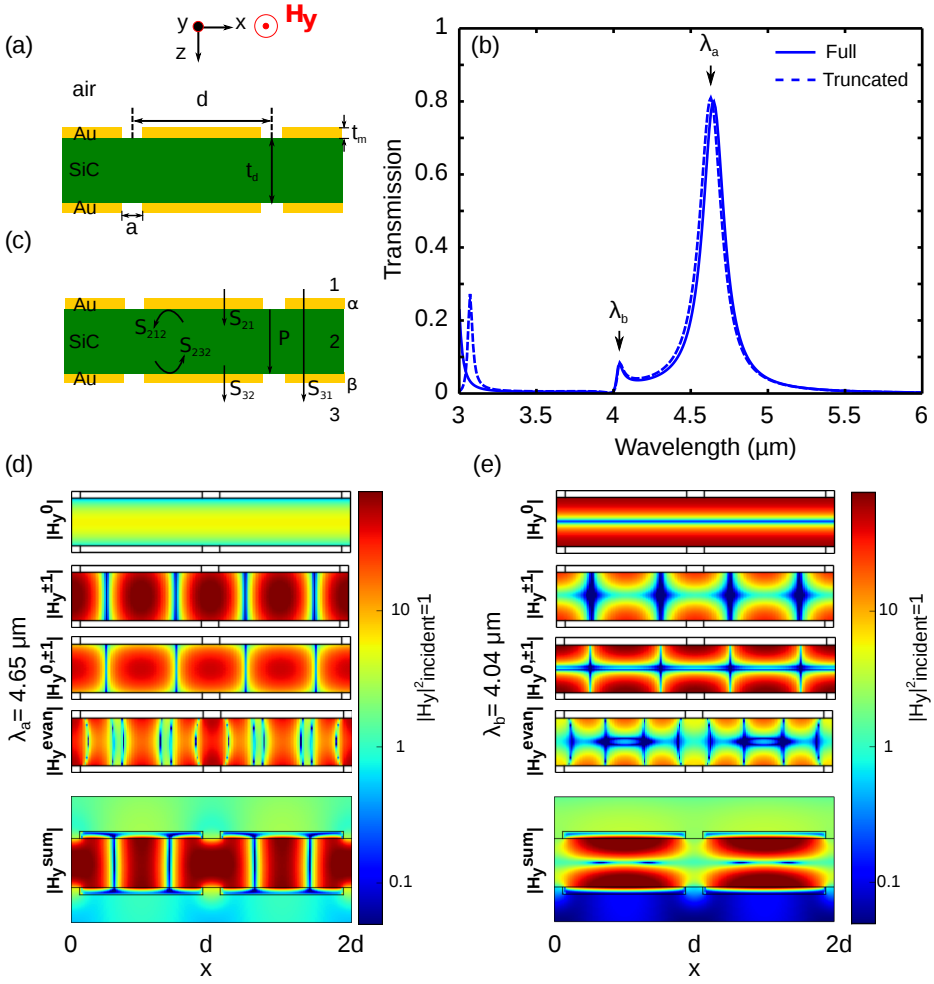

Fig. 1. Optical response of a metal-dielectric GMR filter. (a) Schematic of the freestanding GMR filter (surrounded by air). The geometrical parameters are: grating period $d = 2\ \mu$m, SiC layer thickness $t_d = 700$ nm, metal thickness $t_m = 100$ nm and slit width $a = 250$ nm. (b) Transmission spectra at normal incidence of the metal-dielectric structure considering all the diffracted orders (solid line) and considering only the three first diffracted orders (dashed line). (c) Definition of the S-matrices used for the transmission spectrum calculations. Contour plots of the magnetic field distributions of the overall field $\mathbf{H_y^{sum}}$ and the field contributions $\mathbf{H_y^0}$, $\mathbf{H_y^{\pm 1}}$, $\mathbf{H_y^{0,\pm 1}}$ and $\mathbf{H_y^{evan.}}$: (d) at $\lambda_a = 4.65\ \mu$m and (e) at $\lambda_b = 4.04\ \mu$m.

#246738
Received 24 Jul 2015; revised 11 Oct 2015; accepted 19 Oct 2015; published 30 Nov 2015

2. Matrix formalism

GMRs are based on the coupling of the incident light to a waveguide via diffracted orders created by a periodic grating [15, 16]. In particular ref. [11] shows that the GMR is due to the coupling of the $\pm 1^{st}$ orders diffracted by a metallic grating to the dielectric layer guided-modes. The metal-dielectric GMR structure we consider consists in two identical one-dimensional gold gratings with a silicon carbide (SiC) layer in-between, as depicted on Fig. 1(a). The choice of the geometrical parameters stems from the procedure that was used in refs. [11] and [13] to obtain a transmission peak at 4.65μm. With the following values (grating period $d = 2$ μm, SiC layer thickness $t_d = 700$ nm, metal thickness $t_m = 100$ nm and slit width $a = 250$ nm), we expect a high internal reflectivity of the metallic interfaces for TM-polarized light (with the magnetic field Hy parallel to the slits) [17, 18], and no diffracted order in the 3 to 6 μm spectral range. The thickness t_d is large enough to prevent any coupling of the evanescent waves from the two sides, including when the surface plasmon-polaritons are excited at wavelength close to $dn_d \approx 5.7\mu$m, where n_d the refractive index of the waveguide (2.84 for SiC).

2.1. Resonance analysis

A first transmission spectrum is calculated with the Rigorous Maxwell Constitutive Approximation (RMCA) method [19] considering all the diffracted orders using N mesh points ($N \approx 100$), a SiC permittivity fixed at $\varepsilon_d = 2.84^2$ and a dielectric function of gold given by a Drude model : $\varepsilon_m(\lambda) = 1 - [(\lambda_p/\lambda + i\gamma)\lambda_p/\lambda]^{-1}$ with $\lambda_p = 159$ nm and $\gamma = 0.0048$ [20, 21]. The full-calculation spectrum on Fig. 1(b) exhibits two transmission peaks at $\lambda_a = 4.65$ μm and $\lambda_b = 4.04$ μm. The resonance "b" has a very low intensity compared to the resonance "a" with a transmission up to 80%.

A second transmission spectrum is calculated by considering a smaller number of diffracted orders m, therefore the size of the S-matrices depicted on Fig. 1(c) is reduced. By using the scattering matrix formalism, the transmission amplitude S matrix of the all structure is written

$$S_{31} = S_{32}P^{1/2}(\sum_{k=0}^{\infty}(P^{1/2}S_{212}PS_{232}P^{1/2})^k)P^{1/2}S_{21}, \tag{1}$$

or assuming that the geometrical serie converges

$$S_{31} = S_{32}P^{1/2}(I - P^{1/2}S_{212}PS_{232}P^{1/2})^{-1}P^{1/2}S_{21}, \tag{2}$$

with I being the $m \times m$ identity matrix. The matrices S_{32} and S_{21} describe the transmission of the diffracted orders through the metallic gratings. The order 0 is the only one considered in this calculation, as the only order propagating in the incoming medium 1 and the outcoming medium 3. Thus, the matrice S_{32} is indeed a $1 \times m$ row vector, and the matrice S_{21} a $m \times 1$ column vector. The matrices S_{232} and S_{212} are $m \times m$ square matrices describing the internal scattering of the orders propagating in the medium 2 and reflecting onto the metallic mirrors. $P = (p_{ij})$ is diagonal with its components $p_{jj} = e^{ik_z^{(j)}t_d}$ and $1 \leq j \leq m$; for example $k_z^{(0)}$, $k_z^{(1)}$ et $k_z^{(2)}$ are the propagation constants of the orders 0, $+1$ and -1. Finally, the transmission for the all structure is $T = |S_{31}|^2$.

From now on, we consider the case of normal incidence, for which orders +1 and -1 are excited symmetrically. The truncated response considering only the orders 0, +1 and -1 corresponds to a 2×2 matrix ($m = 2$), and is plotted (dotted line) on Fig. 1(b). It shows a very good agreement with the full calculation. In this approximation, S_{21} and S_{32} are considered as column and row vectors with two components, and P, S_{232} and S_{212} are 2×2 matrices.

On Fig. 1(b), the very good agreement between the exact response and the two-mode model spectrum on the $3.5 - 6\,\mu$m wavelength range demonstrates that only the propagating orders

#246738 Received 24 Jul 2015; revised 11 Oct 2015; accepted 19 Oct 2015; published 30 Nov 2015

play a significant role in the optical response, while evanescent orders have a low influence. In fact, since only the three orders 0, $+1$ and -1 are propagating, all the propagation factors for $j \geq 3$ tend to 0. Accordingly, the discrepancy below $3.5\,\mu$m between the resonance peaks can be corrected by taking the $\pm 2^{nd}$ diffracted orders into account in our simplified model. Figures 1(d) and 1(e) represent the magnetic field distribution over the GMR structure at λ_a and λ_b. The overall magnetic field $\mathbf{H_y^{sum}}$ is compared to the magnetic field contributions $\mathbf{H_y^0}$, $\mathbf{H_y^{\pm 1}}$ and $\mathbf{H_y^{evan.}}$ of the 0^{th} order, the $\pm 1^{st}$ order and the evanescent orders. We also plot the magnetic field contribution $\mathbf{H_y^{0,\pm 1}}$ which corresponds to the interference between the 0^{th} and $\pm 1^{st}$ orders ($\mathbf{H_y^{0,\pm 1}}$ is given by the cross-coupling term appearing when developing the sum $|\mathbf{H_y^0} + \mathbf{H_y^{\pm 1}}|$). At λ_b, the prevalence of the 0^{th} order is due to the Fabry-Perot resonance and therefore explains the intensity distribution of $\mathbf{H_y^{sum}}$: the $x-$invariant $\mathbf{H_y^0}$ field is slightly perturbed by the d-periodic $\mathbf{H_y^{\pm 1}}$ field. At λ_a, the $\pm 1^{st}$ diffracted orders dominate. This is consistent with the observation of a $d/2$-periodic field $\mathbf{H_y^{\pm 1}}$ of the standing-wave resulting from the interference of the d-periodic orders $+1$ and -1. Nonetheless, for the resonance "a" we observe that evanescent orders are quite intense. We can still neglect them because we do not consider their propagation in the SiC layer but take them into account inside the transmission and reflection matrix coefficients. This might yet explain the small difference we see between the two spectra on Fig. 1(a).

2.2. *Scalar expression for the transmission*

The loop matrix $M = P^{1/2} S_{212} P S_{232} P^{1/2}$ is introduced. It refers to all the multiple reflections onto the metallic gratings and the propagation inside the SiC layer of the 0^{th} and $\pm 1^{st}$ diffracted orders. Diagonalizing M allows to write $M = \Pi D \Pi^{-1}$ with $D = \begin{pmatrix} d_a & 0 \\ 0 & d_b \end{pmatrix}$ (Π is a transfer matrix). Finally the Eq, (2) is equivalent to

$$S_{31} = S_{32} P^{1/2} \Pi (I - D)^{-1} \Pi^{-1} P^{1/2} S_{21}. \tag{3}$$

Then setting down $\Pi = \begin{pmatrix} \Pi_{0a} & \Pi_{0b} \\ \Pi_{1a} & \Pi_{1b} \end{pmatrix}$, $\Pi^{-1} = \begin{pmatrix} \Pi_{a0} & \Pi_{a1} \\ \Pi_{b0} & \Pi_{b1} \end{pmatrix}$, $S_{32} = \begin{pmatrix} s_0^\beta & s_1^\beta \end{pmatrix}$, $S_{21} = \begin{pmatrix} s_0^\alpha \\ s_1^\alpha \end{pmatrix}$ and $P^{1/2} = \begin{pmatrix} p_0^{1/2} & 0 \\ 0 & p_1^{1/2} \end{pmatrix}$ (with $p_0 = e^{ik_z^{(0)} t_d}$, $p_1 = e^{ik_z^{(\pm 1)} t_d}$) and developing the Eq. (3), we obtain a scalar expression for the transmission amplitude

$$\begin{aligned} S_{31} = {} & (\Pi_{0a} p_0^{1/2} s_0^\beta + \Pi_{1a} p_1^{1/2} s_1^\beta) \frac{1}{1 - d_a} (\Pi_{a0} p_0^{1/2} s_0^\alpha + \Pi_{a1} p_1^{1/2} s_1^\alpha) \\ & + (\Pi_{0b} p_0^{1/2} s_0^\beta + \Pi_{1b} p_1^{1/2} s_1^\beta) \frac{1}{1 - d_b} (\Pi_{b0} p_0^{1/2} s_0^\alpha + \Pi_{b1} p_1^{1/2} s_1^\alpha) \end{aligned} \tag{4}$$

Figure 2(a) shows that the transmission spectrum can be divided in two parts in agreement with the two-term scalar expression found for the transmission intensity

$$T = |S_{31}|^2 \approx T_a + T_b, \tag{5}$$

where $T_a = |(\Pi_{0a} p_0^{1/2} s_0^\beta + \Pi_{1a} p_1^{1/2} s_1^\beta)(\Pi_{a0} p_0^{1/2} s_0^\alpha + \Pi_{a1} p_1^{1/2} s_1^\alpha)/(1 - d_a)|^2$ and $T_b = |(\Pi_{0b} p_0^{1/2} s_0^\beta + \Pi_{1b} p_1^{1/2} s_1^\beta)(\Pi_{b0} p_0^{1/2} s_0^\alpha + \Pi_{b1} p_1^{1/2} s_1^\alpha)/(1 - d_b)|^2$. T_a approximates well the intensity spectrum around λ_a and T_b around λ_b. We also notice that the transmission peaks appear at λ_a when $\arg(d_a) \equiv 0[2\pi]$ and at λ_b when $\arg(d_b) \equiv 0[2\pi]$ (cf Fig. 2(b)). Therefore the 0^{th} and $\pm 1^{st}$ orders can be viewed as coupled resonators that interfere constructively in the GMR structure when $\arg(d_a) \equiv 0[2\pi]$ or $\arg(d_b) \equiv 0[2\pi]$.

#246738 Received 24 Jul 2015; revised 11 Oct 2015; accepted 19 Oct 2015; published 30 Nov 2015

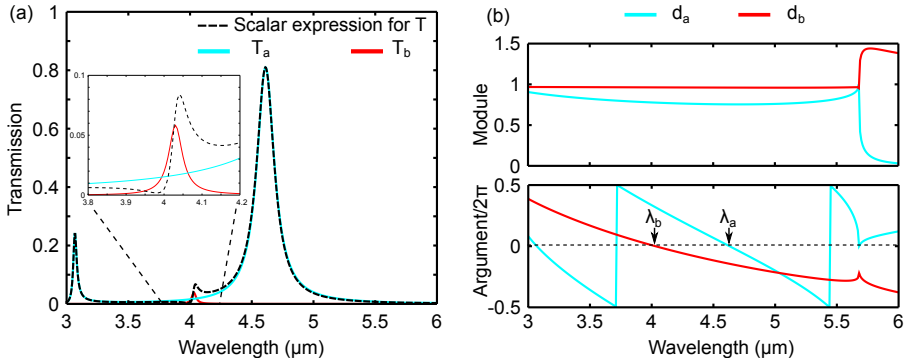

Fig. 2. Scalar expression for the transmitted intensity. (a) Plot of the scalar expression using Eq. (4) (black dashed line) separated in two terms: term proportional to $1/1-d_a$ (light blue line) and term proportional to $1/1-d_b$ (red line). (b) Plot of the two complex eigenvalues d_a and d_b of the loop matrix M.

3. Symmetrisation of guided-mode resonance filters

3.1. Symmetry criterion

We want to study the effect of symmetry on the resonance "a". Although the Fabry-Perot peak corresponds to a single-mode resonance associated to a wavevector k_z, we note two analogies between the Fabry-Perot resonance and the GMR resonance. (i) Considering the expression T_a we note that it is analogous to the classical expression $|t_{32}t_{21}e^{ik_zt_d}/(1-r_{212}r_{232}e^{2ik_zt_d})|^2$ for the intensity transmitted through a Fabry-Perot cavity of thickness t_d as a function of the transmission and reflection Fresnel coefficients t_{32}, t_{21}, r_{212} and r_{232}. (ii) Fabry-Perot resonances occur similarly when $\arg(r_{212}r_{232}e^{2ik_zt_d}) \equiv 0[2\pi]$. For a Fabry-Perot cavity, this condition defines similarly a resonance round trip.

The eigenvalue d_a of the matrix M also turns to be the eigenvalue of $(P^{1/2}S_{212}P^{1/2})(P_2^{1/2}S_{232}P_2^{1/2})$, $P^{1/2}$ and $P_2^{1/2}$ being seen as the propagation matrices related to two dielectric layers of thicknesses t and t_2, given that $t_d = t + t_2$. Finally, as a symmetric Fabry-Perot cavity is defined by $r_{212}e^{ik_zt_d} = r_{232}e^{ik_zt_d}$, we introduce the eigenvalues d_{212} and d_{232} of the matrices $P^{1/2}S_{212}P^{1/2}$ and $P_2^{1/2}S_{232}P_2^{1/2}$. A symmetry criterion is formulated, the necessary condition to obtain a symmetric filter being: $d_{212} = d_{232}$.

3.2. Symmetrisation results and discussions

Figure 3(a) presents three different freestanding GMR structures A, B and C. The structure A is the one originally shown on Fig. 1(a): it is made of two identical periodic gold gratings with a SiC layer in-between. The structure B only differs from A because the slits of the lower grating are filled with SiC. The structure B is therefore not symmetric, and we observe that $d_{212} \neq d_{232}$ (on Fig. 3(b), solid lines refer to d_{212} and dotted lines to d_{232}). To restore the equality, three degrees of freedom are available: the thickness t_2 of the dielectric waveguide lower part and the slit width a_2 and metal thickness t_{m2} of the lower grating. In theory, three parameters are more than enough to make the complex d_{232} equal to d_{212} at the resonance wavelength. For the structure C, the equalization is even obtained on a large wavelength range. As a consequence, the slopes of the arguments of d_{212} and d_{232} also coincide, which allows to restore the same quality factor.

To derive an expression for the quality factor, we consider the denominator of the scalar

#246738 Received 24 Jul 2015; revised 11 Oct 2015; accepted 19 Oct 2015; published 30 Nov 2015

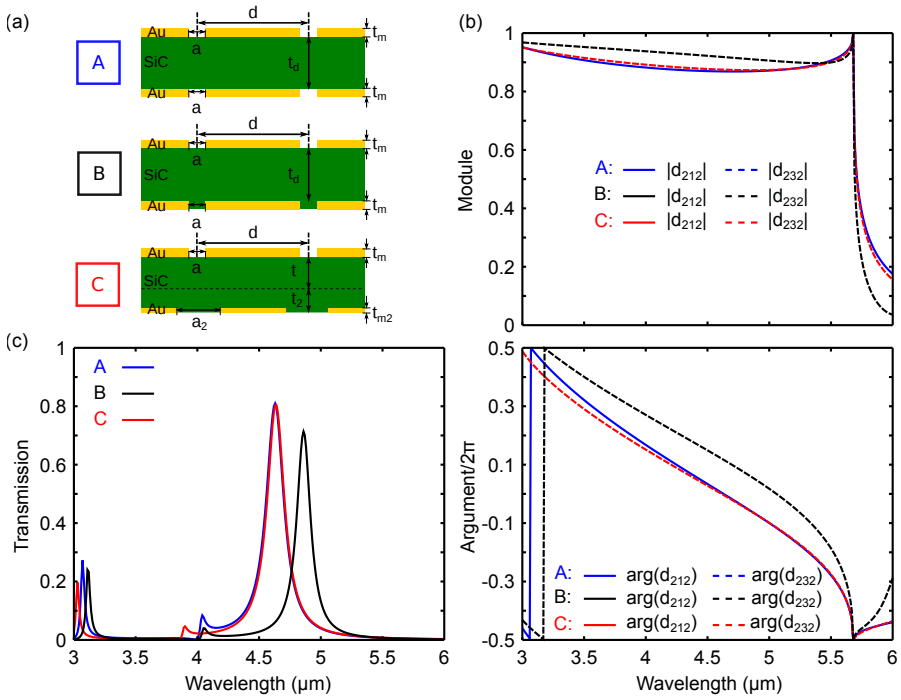

Fig. 3. Validation of the symmetry criterion. (a) Schematic of three freestanding GMR structures A, B and C. For the structures A and B, the gold grating period is $d = 2$ μm, the SiC layer thickness is $t_d = 700$ nm, the gold grating slit width is $a = 250$ nm and the gold grating thickness is $t_m = 100$ nm. For the structure C, the gold grating period is $d = 2$ μm; the SiC layer is divided in two parts of thickness $t = 350$ nm and $t_2 = 320$ nm; the gold gratings are different, the upper one having a thickness $t_m = 100$ nm and a slit width $a = 250$ nm, and the lower one a thickness $t_{m2} = 60$ nm and slit width $a_2 = 350$ nm. (b) Modules and arguments of coefficients d_{212} and d_{232} corresponding to the structures A , B and C. (c) Transmission spectra at normal incidence of the structures A, B and C calculated using Eq. (2).

expression T_a. We introduce the length α by setting down: $d_a = |d_a|e^{i\delta k_a \alpha}$ where $\delta k_a = k_0 - k_a$ with $k_0 = 2\pi/\lambda$ and $k_a = 2\pi/\lambda_a$. Consecutively around the resonance wavelength λ_a, $|1-d_a|^2 \approx (1-|d_a|)^2 + |d_a|\delta k_a^2 \alpha^2$. The quality factor Q being defined as $Q = k_0/2k_{a,1/2}$, the Lorentzian shape of T_a allows to write $|d_a|k_{a,1/2}^2\alpha^2 = (1-|d_a|)^2$. Finally we obtain the following expression for the quality factor

$$Q = \frac{k_0}{2} \cdot \frac{|d_a|^{1/2}}{1-|d_a|}\alpha \tag{6}$$

The length α (resp. β defined similarly by $d_b = |d_b|e^{i\delta k_b \beta}$) can be retrieved numerically, as $\alpha = \delta d_a/\delta k_a$ (we will choose $\delta k_a = k_0/1000$). To understand the origin of phase variations, we derive d_a, considering that $d_a = \Pi_a^{-1}(P^{1/2}S_{212}P^{1/2})(P_2^{1/2}S_{232}P_2^{1/2})\Pi_a$, with $\Pi_a^{-1} = \begin{pmatrix}\Pi_{a0} & \Pi_{a1}\end{pmatrix}$

#246738 Received 24 Jul 2015; revised 11 Oct 2015; accepted 19 Oct 2015; published 30 Nov 2015

and $\Pi_a = \begin{pmatrix} \Pi_{0a} \\ \Pi_{1a} \end{pmatrix}$, and we obtain the first order differential

$$\begin{aligned}
\delta d_a = &(\delta\Pi_a^{-1})P^{1/2}S_{212}P^{1/2}P_2^{1/2}S_{232}P_2^{1/2}\Pi_a \\
&+\Pi_a^{-1}(\delta P^{1/2})S_{212}P^{1/2}P_2^{1/2}S_{232}P_2^{1/2}\Pi_a \\
&+\Pi_a^{-1}P^{1/2}(\delta S_{212})P^{1/2}P_2^{1/2}S_{232}P_2^{1/2}\Pi_a \\
&+\Pi_a^{-1}P^{1/2}S_{212}(\delta P^{1/2})P_2^{1/2}S_{232}P_2^{1/2}\Pi_a \\
&+\Pi_a^{-1}P^{1/2}S_{212}P^{1/2}(\delta P_2^{1/2})S_{232}P_2^{1/2}\Pi_a \\
&+\Pi_a^{-1}P^{1/2}S_{212}P^{1/2}P_2^{1/2}(\delta S_{232})P_2^{1/2}\Pi_a \\
&+\Pi_a^{-1}P^{1/2}S_{212}P^{1/2}P_2^{1/2}S_{232}(\delta P'^{1/2})\Pi_a \\
&+\Pi_a^{-1}P^{1/2}S_{212}P^{1/2}P_2^{1/2}S_{232}P_2^{1/2}(\delta\Pi_a) \\
&+o(\delta d_a).
\end{aligned} \tag{7}$$

These 8 terms have been evaluated numerically. It appears that, contrary to the case of a simple Fabry-Perot filter where the phase variations at reflection onto the mirrors are negligible, the terms $\Pi_a^{-1}P^{1/2}(\delta S_{212})P^{1/2}P_2^{1/2}S_{232}P_2^{1/2}\Pi_a$ and $\Pi_a^{-1}P^{1/2}S_{212}P^{1/2}P_2^{1/2}(\delta S_{232})P_2^{1/2}\Pi_a$ must be taken into account. Furthermore, we notice that the first and last terms of this sum $(\delta\Pi_a^{-1})P^{1/2}S_{212}P^{1/2}P_2^{1/2}S_{232}P_2^{1/2}\Pi_a$ and $\Pi_a^{-1}P^{1/2}S_{212}P^{1/2}P_2^{1/2}S_{232}P_2^{1/2}(\delta\Pi_a)$ are negligible.

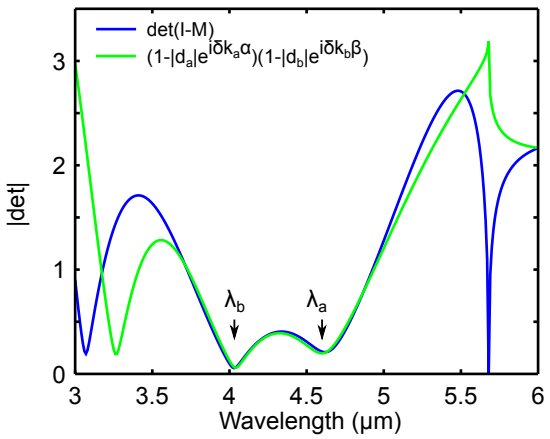

Fig. 4. Determinant as a function of wavelength of the 2×2 matrix $I-M$ compared to the numerically-calculated expression $(1-|d_a|e^{i\delta k_a\alpha})(1-|d_b|e^{i\delta k_b\beta})$.

The eigenmodes complex frequencies ω_a and ω_b are solutions of the implicit equation

$$\det(I-M)=0. \tag{8}$$

These complex values permit to fully characterize the non-conservative open system around a peak wavelength $\lambda = 2\pi c/\omega$: the decay rate of the mode "a" is $\gamma_a = \Im(\omega_a)$ and the quality factor is defined by $Q_a = \Re(\omega_a)/2\gamma_a$ [22, 23]. The expression (6) for the quality factor Q is analogous to the typical quality factor of a Fabry-Perot resonator of thickness t_d filled with a

#246738 Received 24 Jul 2015; revised 11 Oct 2015; accepted 19 Oct 2015; published 30 Nov 2015

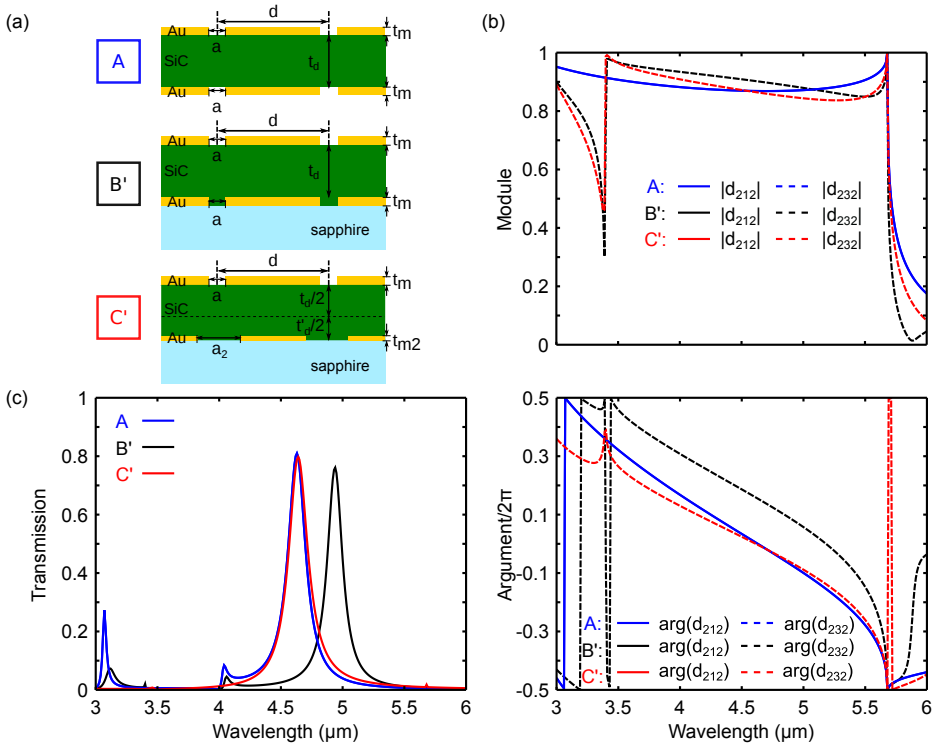

Fig. 5. Symmetrisation of GMR filters on a sapphire substrate of refractive 1.7. (a) Schematic of three GMR structures A, B' and C'. The structure B' has the same geometrical parameters than the structure B. For the structure C', the gold grating period is $d = 2$ μm; the SiC layer is divided in two parts of thickness $t = 350$ nm and $t_2 = 230$ nm; the gold gratings are different, the upper one having a thickness $t_m = 100$ nm and a slit width $a = 250$ nm, and the lower one a thickness $t_{m2} = 50$ nm and slit width $a_2 = 290$ nm. (b) Modules and arguments of coefficients d_{212} and d_{232} corresponding to the structures A , B' and C'. (c) Transmission spectra at normal incidence of the structures A, B' and C' calculated using equation (2).

dielectric of refractive index n_d [24]:

$$Q = \frac{k_0}{2} \cdot \frac{|r|^{1/2}}{1-|r|}(2n_d t_d), \tag{9}$$

given that $r = r_{212}r_{232}$ for highly reflecting interfaces. α is therefore similar to $2n_d t_d$, and can therefore be considered as the cavity optical length.

The assumption that the system is separated in two independent resonators (indexed as a and b) is confirmed by Fig. 4, which shows the exact value of $\det(I-M)$ and the approximated value obtained as the product of terms $(1-d_a)$ and $(1-d_b)$. The two curves are in good agreement over a wide spectral range around the resonance peaks λ_a and λ_b.

Figure 5 shows the result of the symmetrisation approach for a GMR filter on a sapphire substrate. We manage to make d_{212} equal to d_{232} at the resonance wavelength λ_a. This allows to obtain the same transmission maxima for the original freestanding structure A and the structure on substrate C', but not the same quality factor (on Fig. 5 (c) the transmission peak of the structure

#246738 Received 24 Jul 2015; revised 11 Oct 2015; accepted 19 Oct 2015; published 30 Nov 2015

C' appears larger than the one related to the original structure A). The equalization is obtained by enlarging the slits and reducing the thickness of the lower grating. Under these conditions, the hypothesis of a highly reflecting interface and the approximation $-\frac{1}{\ln|r|} \approx \frac{|r|^{1/2}}{1-|r|}$ at first order may no longer be valid, especially as the index contrast between the dielectric waveguide and the sapphire substrate is low. Therefore, second order terms should be considered. Finally, this explains why the the quality factor is not restored in addition to the transmission maximum value at the original resonance wavelength λ_a, even though the symmetry criterion is fulfilled: in this case, the influence of second order terms would require in addition to suppress the small discrepancy we observe on Fig. 5(b) between the slopes of the coefficients d_{212} and d_{232} (both for the modules and arguments), responsible for the slightly lower quality factor we observed for the structure C'.

4. Conclusion

We have proposed a mathematical framework to study the symmetry of metal-dielectric GMR filters. The analysis of the GMR resonance mechanism shows that only the 0^{th} and $\pm 1^{st}$ diffracted orders play a significant role. As a consequence, we can reduce the size of the scattering matrices involved in the RMCA method computation. This reduction allows to write a scalar expression for the intensity transmitted through the GMR structures. A symmetry criterion is then formulated by noticing strong analogies between this expression and the one for standard Fabry-Perot filters. Satisfying this symmetry criterion by adapting the geometrical parameters at the resonance wavelength allows to restore the same transmission maximum value and quality factor than the original symmetric freestanding structure, at the same original resonance wavelength.

This simplification could also be applied to design GMR filters with a large angular acceptance [13], GMR filters exhibiting perfect extinction [25] or for example resonators to be integrated in VCSELs [26, 27], providing the minimum number of electromagnetic modes describing the system is small.

#246738 Received 24 Jul 2015; revised 11 Oct 2015; accepted 19 Oct 2015; published 30 Nov 2015